



Direct Electrochemical Reduction of Mixtures of Iron and Copper Oxides

Hamid Khanmohammadi and Mehdi Ojaghi-Ilkhchi 

Submitted: 1 January 2021 / Revised: 21 June 2021 / Accepted: 2 July 2021 / Published online: 17 August 2021

The direct electrochemical reduction of a mixture of iron and copper oxides in molten salt (calcium chloride) has been performed to investigate the possibility of iron and copper alloy production. To this end, oxide pellets were prepared with a $\text{Fe}_2\text{O}_3\text{:CuO}$ molar ratio of 1:2. To prepare samples with different porosity, an appropriate amount of ammonium bicarbonate was added to the oxide mixture. Pellets sintered at 900 °C for 4 hours. Then electrolysis was conducted at different times (30, 60, 90, and 120 minutes) on oxide cathodes with different porosities (40, 60, and 70%) at constant temperature and voltage (820 °C and 3 V). During electrolysis, the applied electrical current was recorded to determine the degree of reduction. Finally, reduced pellets were characterized using x-ray diffraction (XRD) analysis. The results showed that the degree of reduction of $\text{Fe}_2\text{O}_3\text{-CuO}$ mixture decreases with increasing pellet porosity, and the highest reduction degree takes place for the sample with 40% porosity. XRD patterns of the products showed that more electrolysis time results in more reduction of iron and copper oxide mixtures to metallic iron and copper mixtures.

Keywords copper oxide, direct electroreduction, iron oxide, molten salt, porosity

1. Introduction

Fe-Cu alloys have a metastable miscibility gap in the molten state and have minimal solubility in the solid state (Ref 1). On the other hand, iron and copper alloys have good magnetic properties, high thermal and electrical conductivity, high strength, and good solar absorption (Ref 2–6). Iron-copper alloys are used in contactors, contact bridging, vacuum equipment (Ref 7), lead-frames (Ref 8, 9), solar absorbers (Ref 5), connectors, semiconductor pins, and power sockets (Ref 6). Also, they are used as master alloys to improve the corrosion resistivity of copper and nickel alloys and the mechanical properties of low alloyed coppers as well for grain refining of some brass alloys and aluminum bronze (Ref 10). Advantages of Fe-Cu alloys include low cost, abundance, and availability of these metals compared to other metals such as silver, niobium, tungsten, and chromium (Ref 4).

Owing to their unique properties, these alloys have attracted attention from many researchers in recent decades and are produced as supersaturated solid solutions and eventually metastable alloys by non-equilibrium methods such as mechanical alloying (MA), rapid solidification, sputtering, electrodeposition, and severe plastic deformation (SPD) (Ref 5, 11, 12). Alami et al. (Ref 5) mixed high purity iron and copper powders by mechanical alloying to achieve a 50:50 (wt%) composition and reported the formation of a Cu (Fe) solid solution with a FCC

structure after milling for 6 hours. In addition, Ino et al. (Ref 13) formed the FCC ferromagnetic solid solution using mechanical alloying in the iron and copper binary system with less than 60 wt% iron. Chen et al. (Ref 14, 15) produced a Fe-4%Cu alloy through melting and rapid solidification. Langier et al. (Ref 16) studied the processing of a layered Fe-Cu alloy using pulsed magnetron sputtering (PMS) and impulse plasma deposition (IPD). The results showed that two polycrystalline phases (FCC-Cu and BCC-Fe) are obtained by PMS method, which indicates that there is no mixing of iron and copper atoms. While the deposition of Fe-Cu layers using the IPD method shows the presence of non-equilibrium single-phase supersaturated solid solution (FCC-Cu (Fe) or BCC-Fe (Cu)). Sarac and Baykul (Ref 17) electrodeposited the Fe-Cu film on indium-tin oxide substrate in an electrolyte with different concentrations of iron (0.02, 0.04, and 0.08 M), and the same concentration of copper sulfate and boric acid (0.01 M). It was found that various concentrations of iron ion in the electrolyte had a great influence on the chemical composition, surface morphology, and microstructural properties of the Fe-Cu films. Bachmaier et al. (Ref 2) processed the Fe-Cu alloy using two-stage high-pressure torsion on various $\text{Fe}_{100-X}\text{-Cu}_X$ compounds ($X = 15, 50, 70, 85$). Yang et al. (Ref 18) developed a multi-layered iron and copper composite by accumulative roll bending. Shingu et al. (Ref 19) produced a multi-layered iron and copper bulk material in nanoscale using repeated pressing and rolling processes.

The FFC Cambridge process, invented by Fray, Farthing, and Chen (Ref 20), is a technique based on direct electrochemical reduction of oxides or other compounds (especially more stable compounds such as TiO_2 , SiO_2 , Nb_2O_5) as single or mixture to their respective metals or alloys in a molten salt electrolyte (usually CaCl_2). Compared to the conventional metal extraction processes, this approach offers the advantages of process simplicity and fastness, as well lower cost and higher quality of the product. In the case of oxides, it is assumed that the electro-deoxidation stages include oxygen ionization in a solid oxide cathode, its dissolution in the molten salt electrolyte, its migration toward the anode under the applied

Hamid Khanmohammadi and Mehdi Ojaghi-Ilkhchi, Faculty of Materials Engineering, Research Center of Advanced Materials, Sahand University of Technology, 5331817634 Sahand New Town, Tabriz, Iran. Contact e-mail: m_ojaghi@sut.ac.ir

electrical potential, and its discharging on the anode. Oxygen forms carbon dioxide and carbon monoxide in the graphite anode and it evolves as gaseous oxygen in neutral anodes. The applied cell potential is lower than the molten salt reversible decomposition potential, and the amount of oxygen removal in this process generally depends on the potential and duration of the electrolysis process (Ref 21).

To produce the alloy, metal oxides can be mixed with the desired ratio and used as the cathode. As the oxygen removal from mixed oxides occurs, the metals are combined as desired alloy or intermetallic. This type of alloying, without the melting of the relevant metals, has many advantages over common methods, including the feasibility of alloying of metals with significantly different melting points and that of metals which their alloying are impossible by conventional techniques, as well solving of problems such as segregation and oxidation of reactive metals. The oxides of Ni, Ce, Hf, U, Zr, Nb, V, Fe, Cr, B, Al, or their mixtures have been reduced, and many alloys, such as Ti-Al, Ti-Al-V, Ti-Ni, Fe-Ti, and Nb₃Sn, have been produced in the laboratory scale using FFC process. Also, it seems that most metal carbides can be produced by the FFC method (Ref 21).

Gordo et al. (Ref 22) studied the preparation conditions of chromium oxide pellets and the effect of sintering temperature on the porosity of the pellet. Dai et al. (Ref 23) investigated the effect of sintering temperature on the production of CeCo₅ alloy using the FFC process and showed that increasing sintering temperatures result in poor reduction efficiency. In the electroreduction process, the electrolyte composition influences the reduction rate and the product quality. Calcium chloride and sodium chloride are most commonly used in the FFC process, and their eutectic composition is used to decrease the reduction temperature and energy consumption. Zhao et al. (Ref 24) studied the effect of electrolyte temperature on reducing a mixture of cerium and nickel oxides and concluded that by increasing the temperature of the molten salt, higher reaction rates could be achieved. The applied voltage is another influential factor on the process rate, which its increasing leads to higher reduction rates. On the other hand, higher applied voltage results in more energy consumption, and decreased current efficiency. Therefore, an optimum level of voltage will be industrially essential. Zhu et al. (Ref 25) studied the effect of voltage on the reduction of nickel oxide and titanium oxide mixtures and showed that by increasing voltage to 2.6 and 2.9 V, the amount of Ti-Ni increased, and some Ni₃Ti phase was observed. By increasing the reduction time, the extent of reduction increases. However, for energy savings, the operation must continue to an optimal time depending on the oxide used as a cathode. Ors et al. (Ref 26) studied the impact of electroreduction time on the processing of Fe-4.6 wt% B. Their findings show that after 12 hours of reduction, the oxide pellets are wholly reduced and converted into a combination of Fe and Fe₂B.

Non-equilibrium methods for the processing of metastable Fe-Cu alloy require high energy and costs. On the other hand, pure iron and copper elements, which are used in these methods, are more expensive than related oxides. Also, there is the possibility of their oxidation and contamination during the production of alloys. Regarding the advantages of the direct electrochemical reduction method in terms of simplicity and the use of cheap oxide compounds (relative to pure elements), the direct electrochemical reduction of a mixture of iron and copper oxides in molten salt (calcium chloride) has been carried out in this research.

2. Experimental

2.1 Materials

Fe₂O₃ powder (hematite, extra pure, Scharlu, ≤ 1 μm) and CuO (tenorite, extra pure, Scharlu, 5-15 μm) were used to prepare oxide pellets. The SEM images with related EDS analysis of the powders are shown in Fig. 1. Anhydrous CaCl₂ powder (extra pure, Scharlu) as an electrolyte and ammonium bicarbonate powder (extra pure, DAEGUNG) in different ratios (weight ratios of ammonium bicarbonate to the pellet of 0.25: 1 and 0.5: 1) to increase the porosity of pellets were used.

2.2 Preparation of Oxide Pellets

The required amounts of powders with a Fe₂O₃:CuO molar ratio of 1:2 (equal weight ratio of 1:1) were weighed and poured into the plastic container along with a number of hardened chromium balls (10 mm in diameter, the ball to powder weight ratio of 1:1). The enclosed container was manually shaken for 30 minutes to mix the powders homogeneously. The desired amount of mixed powder (about 0.65 g) was weighed and poured into a steel mold (10 mm in diameter), and pressed under uniaxial pressure of 70 MPa. The prepared oxide pellets were sintered at 900 °C for 4 hours under an air atmosphere to enhance their strength. Then the porosity of sintered pellets was measured by the Archimedes method. The approximate dimensions and porosity of the pellets prepared are presented in Table 1.

Figure 2 shows SEM images of the prepared pellets before and after the sintering. As it is seen, the particles were coarser after sintering, which is a result of decreased pellet porosity from about 55% to 40%. According to the map analysis on the SEM image of the sintered pellet (Fig. 3), all elements were uniformly distributed in the sintered pellets, indicating the proper mixing conditions of the powders.

2.3 The Setup and Procedure of Direct Electrochemical Reduction

An alumina crucible (external height of 7 cm, inner height of 6.5 cm, outer diameter of 6 cm, and inner diameter of 5.5 cm) was used as a container for molten calcium chloride electrolyte. A 310 stainless steel tube (height of 60 cm, outer diameter of 7.8 cm, and internal diameter of 6.8 cm) was used as the reactor chamber. A Teflon (PTFE) cap with four holes (two holes of 4 mm in diameter for anode and cathode rods, two others of 6 mm in diameter for gas in and out) was put on the steel chamber (see Fig. 4a). A graphite rod (15 cm in height and 13 mm in diameter, Alfa Aesar) connected to a Kanthal rod (3.5 mm in diameter and 45 cm in length) was used as the anode. As shown in Fig. 4b, the oxide pellet was put on a small sheet of nickel previously welded to a Kanthal rod (3.5 mm in diameter, 60 cm in length) and wrapped by Kanthal wire (0.15 mm in diameter) to enhance the electrolyte, cathode, and electrical conductor triple points. The reactor was placed in a vertical cylindrical resistance furnace. The experimental setup schematic is shown in Fig. 5.

120 g of calcium chloride was put in an alumina crucible, and the crucible was placed inside the steel chamber. Then the Teflon cap was put on the steel chamber, while the anode and cathode were hanging on the top of the crucible. The furnace was heated to 400 °C at 5 °C/min, kept at this temperature for

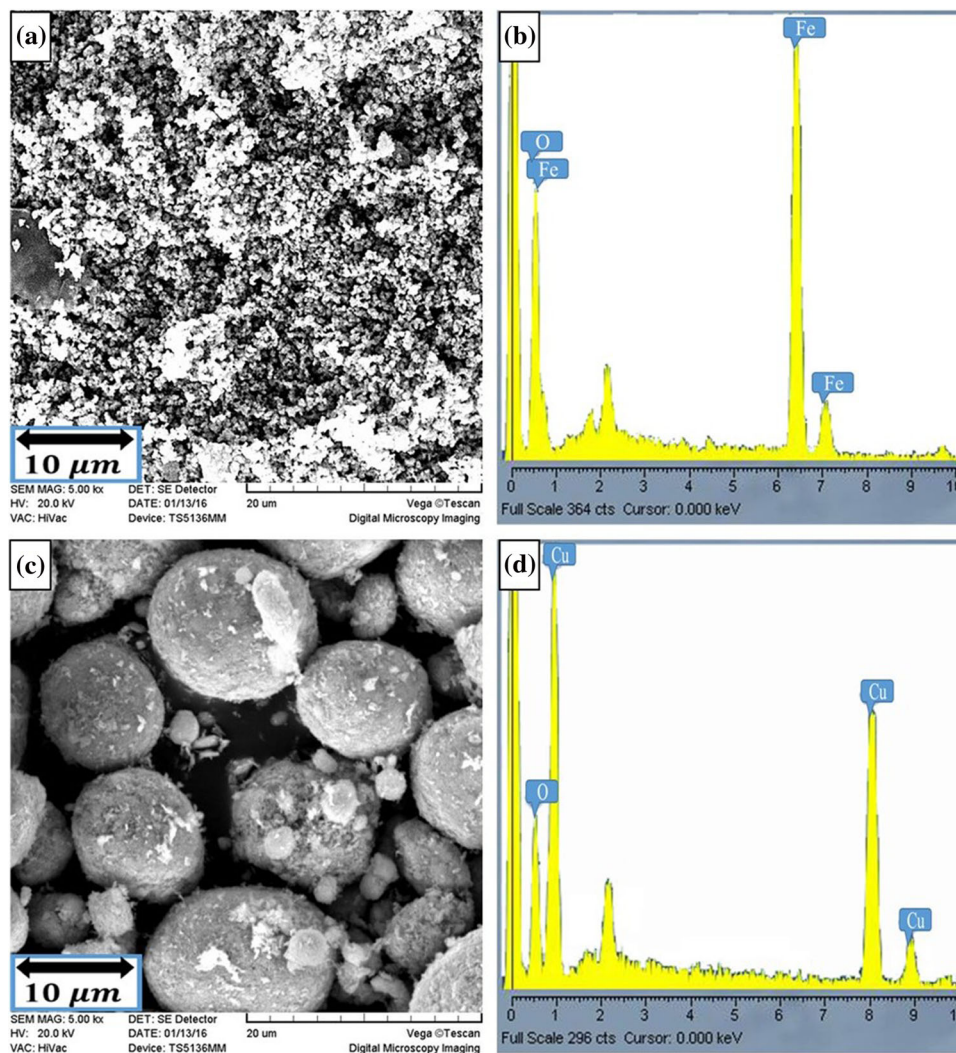


Fig. 1 SEM image and EDS analysis of iron oxide (a and b) and copper oxide (c and d) powders

Table 1 Dimensions and porosity of prepared pellets

Weight ratio of ammonium bicarbonate to pellet	Pellet thickness, mm	Pellet diameter, mm	Porosity, %
0	2–3	10	40
0.25:1	3–4	10	60
0.5:1	4–5	10	70

one hour to ensure salt drying, then warmed to 820 °C at the same rate. After stabilization of the temperature, the cathode and anode were immersed in the molten electrolyte. Then by applying a 3 V electrical potential difference between anode and cathode, the electrolysis began at 820 °C. In order to investigate the effect of reduction time, electrolysis was performed for 30, 60, 90, and 120 min on pellets with ~40% porosity. Also, to evaluate the effect of porosity, electrolysis was carried out for 90 min on pellets with different porosities. In all experiments, argon gas (purity of 99%) flowed at a rate of 150–200 mL/min during electrolysis. Electrical current was automatically recorded at 10 sec intervals during each test to plot the current versus time graphs.

At the end of the electrolysis time, the electrodes were removed from the molten electrolyte and cooled to ambient temperature under the argon gas flow. The reduced pellets were first washed in a diluted HCl solution and then in distilled water for salt removal. Then the pellets were dried and prepared for microstructural and characterization studies.

2.4 Characterization of Raw Materials and Reduction Products

The morphology of the initial oxide powders and oxide pellets was investigated using SEM (Cam Scan model MV300) equipped with EDS. Map analysis on the SEM image of pellets was performed to determine the distribution of elements (Cu,

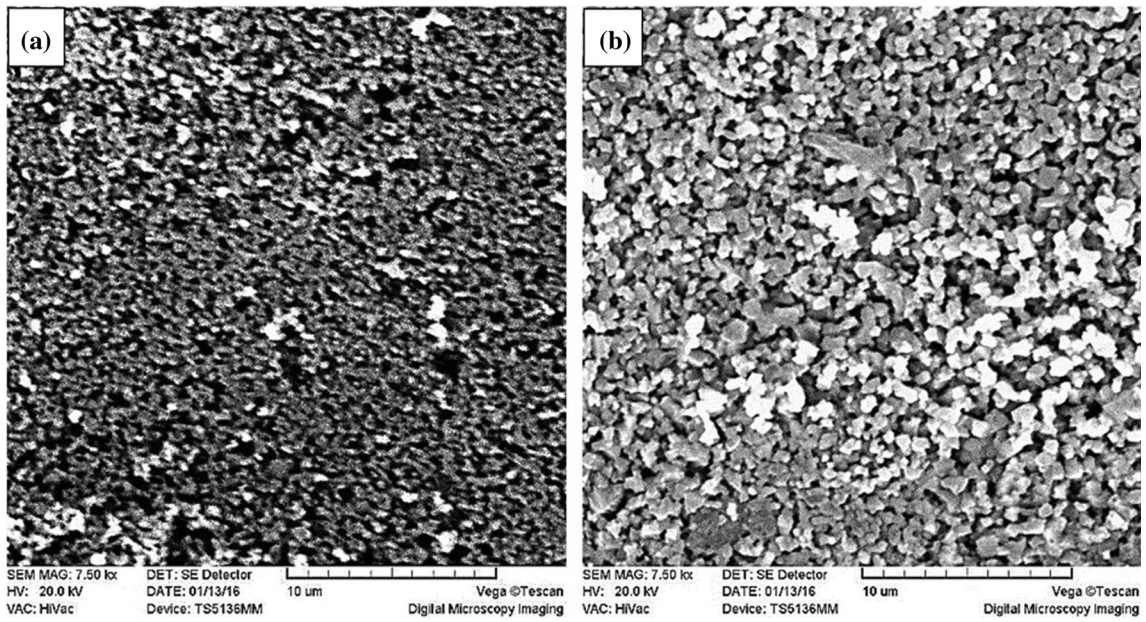


Fig. 2 SEM images of a mixture of iron and copper oxides pellet; before (a) and after sintering (b)

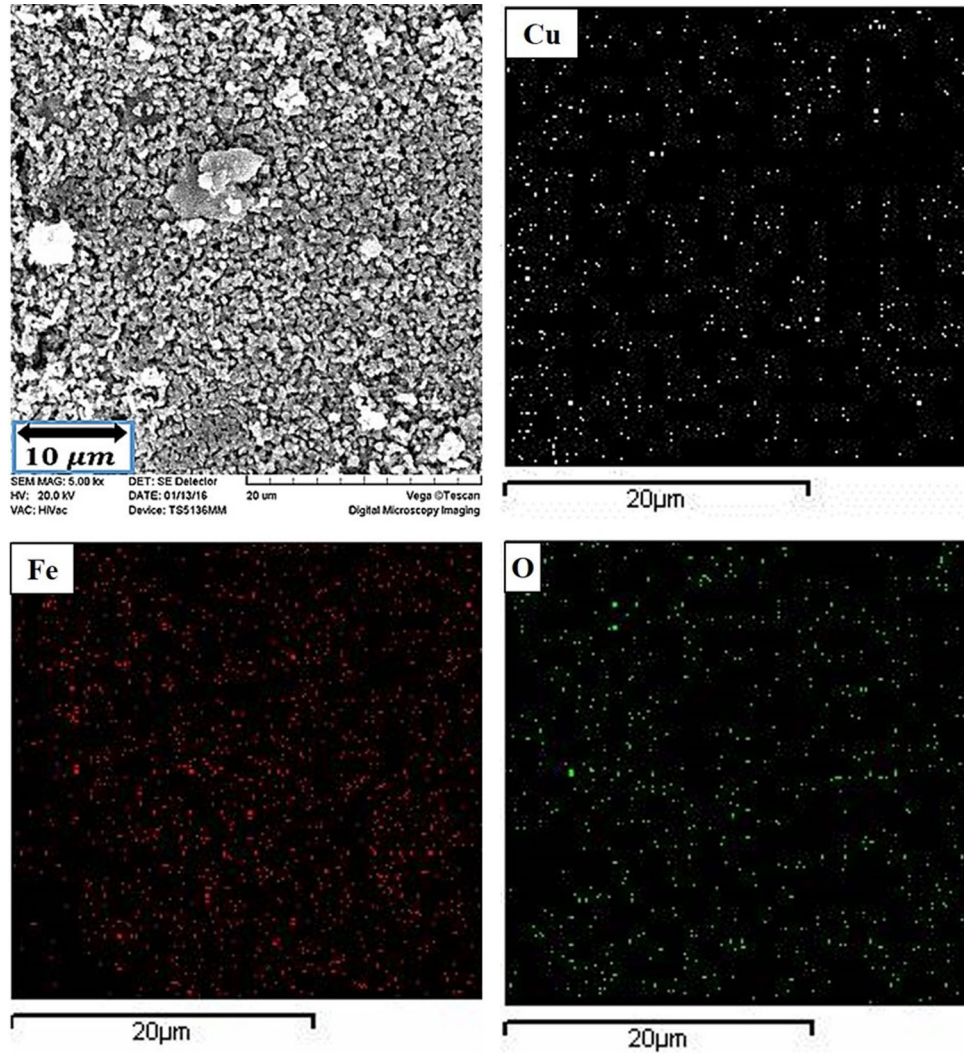


Fig. 3 SEM image and map analysis of the sintered pellet

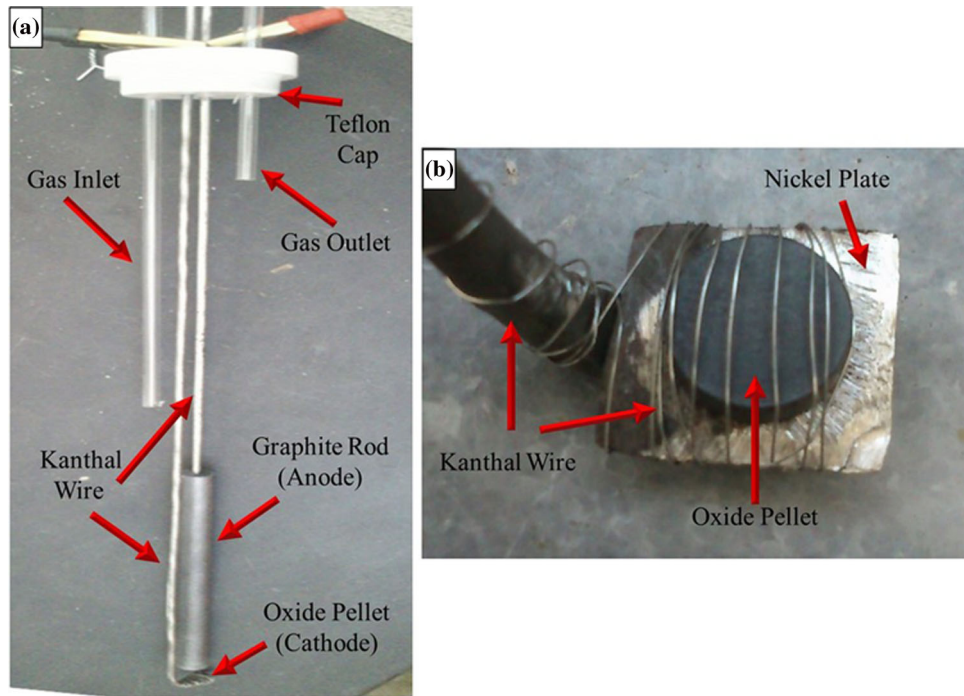


Fig. 4 (a) Teflon cap, graphite rod (anode), oxide cathode, gas in and out pipes, (b) The Kanthal wire wrapped oxide pellet (cathode) on the nickel plate

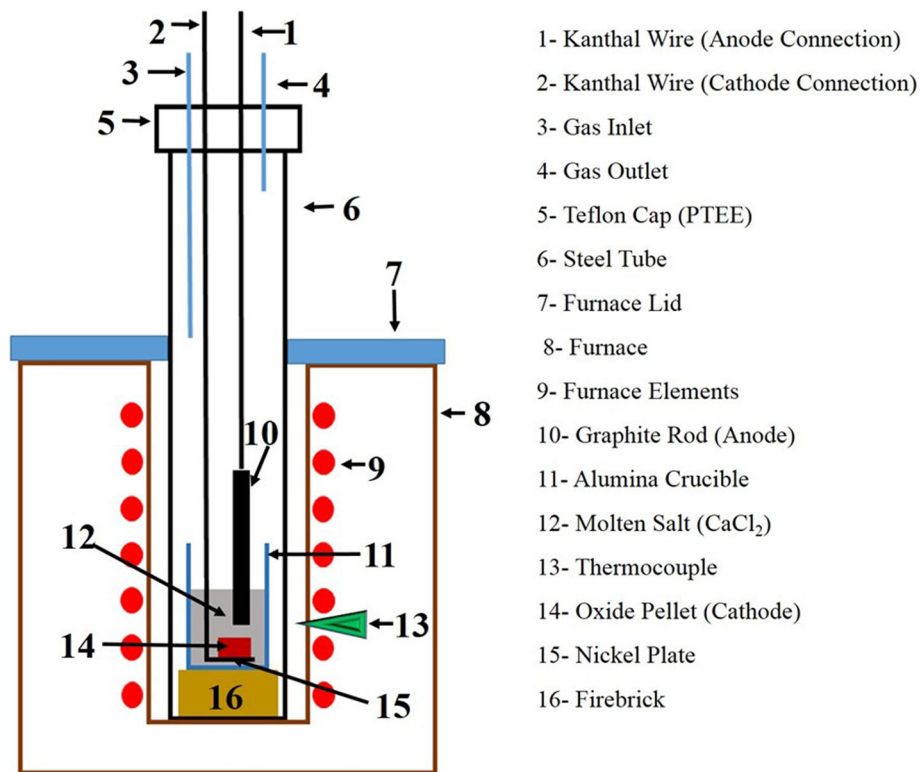


Fig. 5 Schematic presentation of the experimental setup

Fe, and O). Also, XRD of the primary and reduced pellets were prepared by Bruker diffractometer (D8 advanced model) under Cu $\kappa\alpha$ radiation ($\lambda = 1.1541$ nm), the voltage of 40 kV, and current of 40 mA.

3. Results and Discussion

3.1 Reduction Time

The XRD patterns of the pellets before and after reduction for 30, 60, 90, and 120 min are presented in Fig. 6. As shown in the XRD pattern of unreduced pellet, the detected phases are CuFe_2O_4 , CuO , and Fe_2O_3 . In the pellet reduced for 30 min, although the major phases are the same as the unreduced pellet, some peaks of Fe (BCC) and Cu (FCC) are also detected. After reduction for 60 min, the number of peaks was decreased for oxide compounds, whereas sharper Cu (FCC) and Fe (BCC) peaks were increased. As a result, a reduction for 60 min is not adequate to reach the desired amount of the metallic structure.

Only the peaks of Fe (BCC) and Cu (FCC) are observed in the XRD patterns of the samples reduced for 90 and 120 min, and that of the oxide compounds are not detected, which indicates the removal of more oxygen and the reduction of iron and copper oxides to iron and copper. Also, it is observed that by increasing the reduction time from 90 to 120 min, the intensity of Fe (BCC) peaks is increased compared to that of Cu (FCC) peaks, which can be attributed to the diffusion of Cu (FCC) in the Fe (BCC) phase and the formation of a solid solution with a BCC structure. Similar solid solution structures in the Fe-Cu system were reported by other researchers, for example, Cu (Fe) solid solution by Alami et al. (Ref 5), a BCC solid solution by Chen et al. (Ref 14, 15), and non-equilibrium single-phase supersaturated solid solution (FCC-Cu (Fe) or BCC-Fe (Cu)) by Langier et al. (Ref 16). In conclusion, by increasing the reduction time, the reduction of iron-copper

oxides increases; however, the possibility of the formation of solid solution is also increased. The pellets reduced for 30 and 60 min have no metallic luster, and no significant difference is observed with the unreduced pellet. Most of the surfaces of the pellets reduced for 90 min have metallic appearance, and the pellet reduced for 120 min displays more metallic luster.

The current vs. time diagrams plotted during the electrolysis of oxide pellets are presented in Fig. 7. Similar results were reported by Zhao et al. (Ref 24), where a 3-step regime can be considered for the current variations. It includes initial quick raising (once the voltage is applied), relative fast falling during less than 20 min, and gradually decreasing to a relatively stable state as a current plateau is reached. The initial current increase is attributed to the initiation of the reaction at the three phases interlines of the conductor-oxide-electrolyte (the connecting points of the oxide cathode to wrapped Kanthal wire) and its propagation on the surface of the pellet. By progressing the reduction reaction across lower pellet layers, the current drop in the diagrams occurs, indicating a slow reduction due to longer path of oxygen ions diffusion (Ref 27, 28). Finally, the current plateau is related to the continued reduction of inner layers of the pellet by mass transport of ions through molten salt penetrated in metalized porous layers toward the surface of the pellet (bulk electrolyte) (Ref 29). Extending the reduction time (in the range of current plateau) results in decreased residual oxygen content, which varies from less than 10% oxygen to a negligible extent. This results in the coarsening of the metal particles that have been reduced at the early stages of step 3 and the formation of the alloy too (Ref 30).

According to Faraday's law (Eq. 1), the mass of ionized oxygen in electrolysis is proportional to the amount of passed electrical current.

$$m = \frac{MIt}{nF} \quad (\text{Eq 1})$$

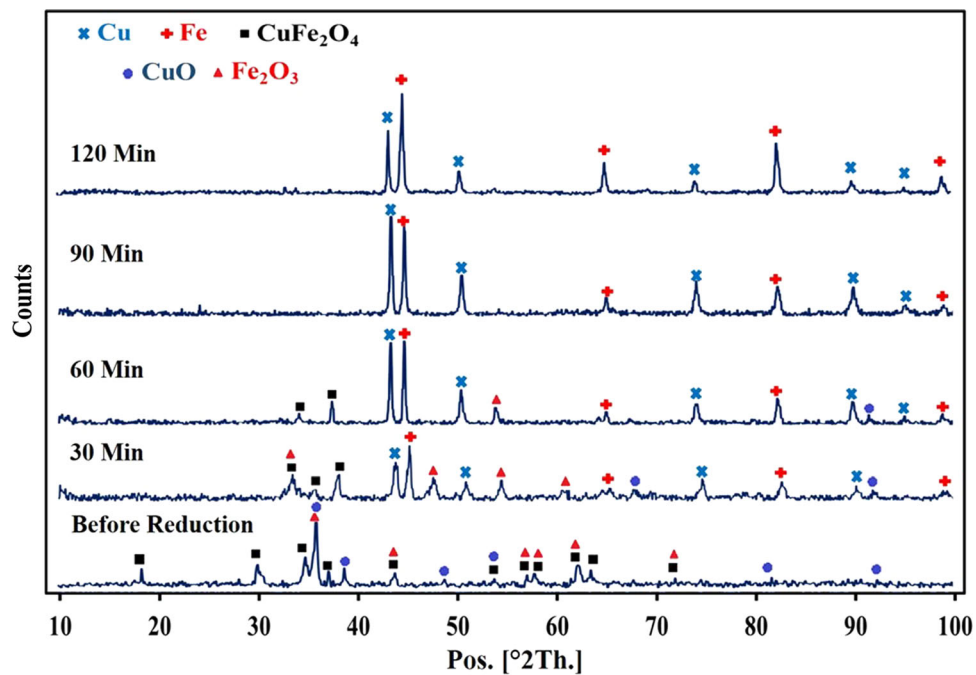


Fig. 6 XRD patterns of the pellets before and after reduction for different periods

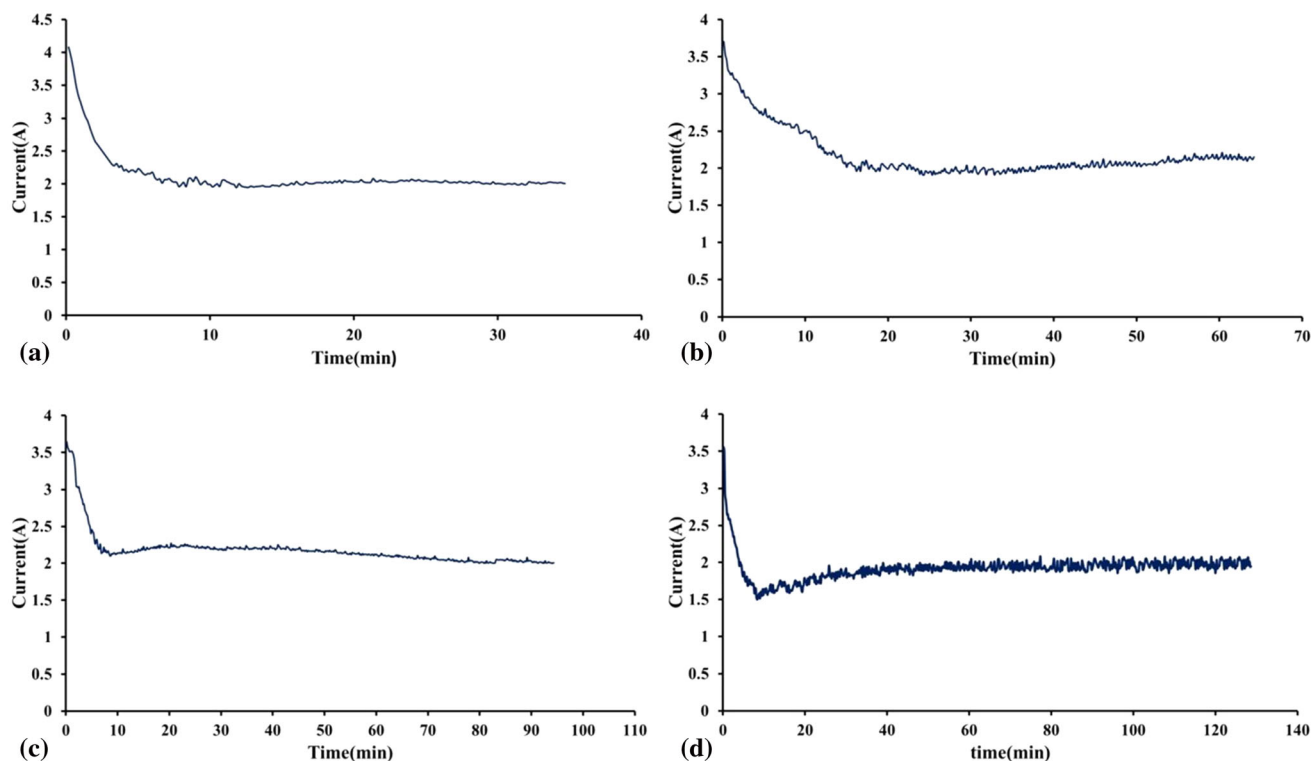


Fig. 7 The variation of current vs. time during the electroreduction of pellets at 820 °C and 3 V for (a) 30, (b) 60, (c) 90, and (d) 120 min

where m is the mass of ionized oxygen (g), M is the molar mass of oxygen (equal to 16), I is the electrical current (A), t is the electrolysis time (s), n is the electrical capacity of oxygen (equal to 2), and F is the Faraday constant (equal to 96500 Coulomb/mole).

The passed charge ($I.t$) can be estimated by calculating the area under the current-time diagram, and consequently, the amount of ionized oxygen (m) is approximately calculated according to Eq. 1, assuming the current efficiency of 100%. The amounts of the calculated area and corresponding ionized oxygen (m) are listed in Table 2 for pellets reduced at different electrolysis times. The data indicated that extending the electrolysis time leads to more significant values of $I.t$ and the mass of ionized oxygen, and consequently, the progress of reduction is increased, confirming the XRD patterns of reduced pellets (Fig. 6).

3.2 Oxide Pellet Porosity

XRD patterns of the pellets of various porosities, electrolyzed at 820 °C and 3 V for 90 min, are demonstrated in Fig. 8. Some peaks of oxide compounds have been detected in the pattern of the more porous pellet (70% porosity), while it is limited to Fe_2O_3 peak at pellet with 60% porosity and finally vanished in the case of the pellet having 40% porosity. Also, the intensity of Fe (BCC) and Cu (FCC) peaks in the pellet containing 60% porosity is lower than that of the less porous pellet (40% porosity). Thus, it can be concluded that lower porosity of pellet corresponds to a higher degree of reduction. The metallic luster of the reduced pellet is decreased by increasing the porosity of the pellet.

Figure 9 shows the $I-t$ diagrams plotted during electrolysis of the pellets with different porosities for 90 min at 820 °C and 3 V. Despite the similar trend of the current variations versus

Table 2 Calculated values of $I.t$ and m for reduced pellets at different reduction times

Reduction time, min	The area under $I-t$ curves (Coulomb)	Ionized oxygen, g
30	4520	0.38
60	8220	0.7
90	11600	0.96
120	14000	1.15

time, the amount of initial current decreases with increasing the porosity of the oxide pellet, and its further lowering occurs in the subsequent stages of the process. The values of calculated $I.t$ and m for the pellets containing various porosities are presented in Table 3. The results reveal that the values are decreased with increasing the porosity of the pellet, confirming the former result observed from XRD patterns. According to the results, with increasing porosity, it will be more difficult to achieve more significant reduction in a shorter time, and longer times will be needed, which in turn will increase the energy consumption and thereby questioning the feasibility of the process.

The lower degree of the reduction with increasing the porosity of the pellet can be explained by the increased distance between the oxide particles and, consequently, the discontinuity of the particles reduced in the initial minutes of the electrolysis. These particles provide a vital path for charge transfer from the wrapped Kanthal wire toward unreduced particles, thereby decreasing the continuity of the reduced particles leads to the lower rate of electrical charge transfer in the pellet and hence decreased degree of reduction. Yasuda et al. (Ref 31) showed that the reduction rate of the dense pellet of SiO_2 is higher than that of the SiO_2 pellet containing more than 60% porosity. Also,

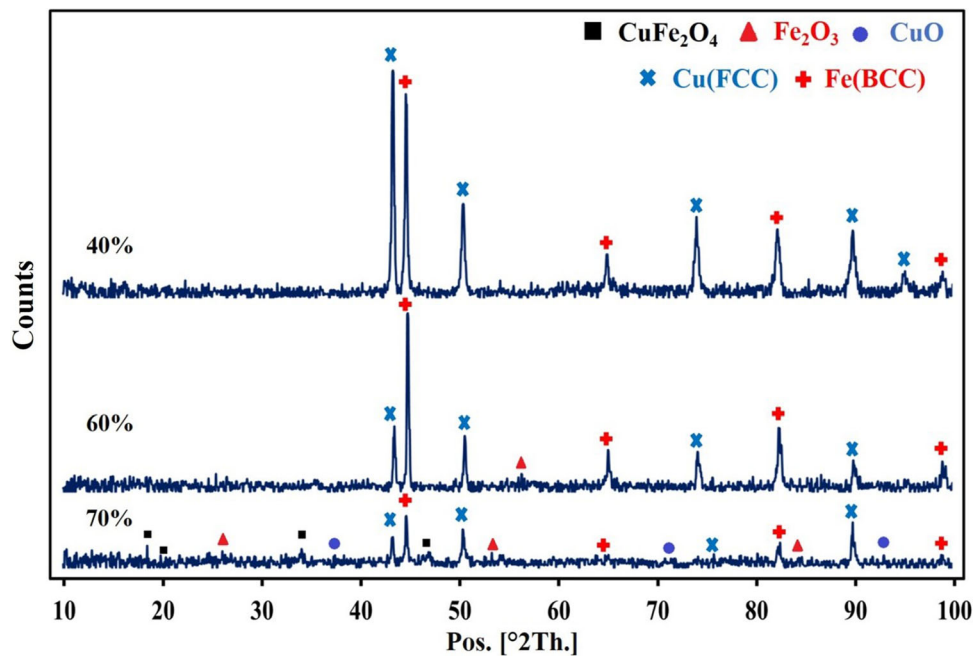


Fig. 8 XRD patterns of pellets containing different porosities reduced at 820 °C, 3 V, 90 min

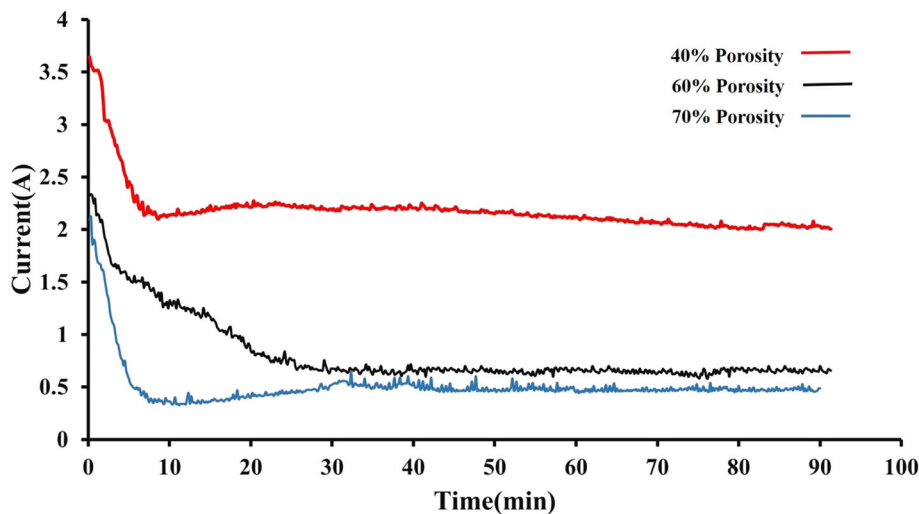


Fig. 9 Current versus time diagrams for reduced pellets of different porosities

Table 3 Calculated values of I.t and m for electrolyzed pellets containing various porosities

Porosity, %	The area under I-t curves (Coulomb)	Ionized oxygen, g
40	11600	0.96
60	4890	0.4
70	3390	0.3

simulation of the electroreduction of the porous oxide pellets revealed that the maximum degree of the reduction is achieved at pellets containing an optimal amount of porosity, so the pellets of upper porosities result in a lower degree of reduction (Ref 32).

According to the results, it can be stated that the amount of porosity of the oxide pellet has a meaningful effect on the reduction, and higher porosity corresponds to a lower degree of direct electroreduction.

4. Conclusion

The direct electrochemical reduction of a mixture of iron and copper oxides in molten salt (calcium chloride) has been investigated. In order to evaluate the effect of the electrolysis time and pellets porosity, the electroreduction experiments were done on pellets of Fe₂O₃:CuO at a molar ratio of 1:2, containing different porosities, at 820 °C under the electrical potential of 3 V for various times. The results showed that the

reduction of a mixture of iron and copper oxides increased with extending the electrolysis time. Also, the direct electrochemical reduction of the mixture of Fe-Cu oxides decreased with increasing the porosity of the pellet, and the maximum reduction value was obtained in the pellet with 40% porosity. Regarding the promising results, further investigations on the product microstructures and properties will be required.

Acknowledgments

This work was financially supported by the Sahand University of Technology under the Grant Number of 30/19763.

References

- F. Dai, C. Cao and B. Wei, Phase Separation And Rapid Solidification of Liquid $\text{Cu}_{60}\text{Fe}_{30}\text{Co}_{10}$ Ternary Peritectic Alloy, *Sci. China Ser. G*, 2007, **50**, p 509–518. <https://doi.org/10.1007/s11433-007-0047-5>
- A. Bachmaier, M. Kerber, D. Setman and R. Pippan, The Formation of Supersaturated Solid Solutions in Fe–Cu Alloys Deformed by High-Pressure Torsion, *Acta Mater.*, 2012, **60**, p 860–871. <https://doi.org/10.1016/j.actamat.2011.10.044>
- J. He, J.Z. Zhao and L. Ratke, Solidification Microstructure and Dynamics of Metastable Phase Transformation in Undercooled Liquid Cu–Fe Alloys, *Acta Mater.*, 2006, **54**, p 1749–1757. <https://doi.org/10.1016/j.actamat.2005.12.023>
- L. Fu, J. Yang, Q. Bi and W. Liu, Combustion Synthesis Immiscible Nanostructured Fe–Cu Alloy, *J. Alloy. Compd.*, 2009, **482**, p L22–L24. <https://doi.org/10.1016/j.jallcom.2009.04.016>
- A.H. Alami, A. Alketbi and M. Almheiri, Synthesis and Microstructural and Optical Characterization of Fe–Cu Metastable Alloys for Enhanced Solar Thermal Absorption, *Energy Procedia*, 2015, **75**, p 410–416. <https://doi.org/10.1016/j.egypro.2015.07.405>
- H. Zhang, H. Zhang and L. Li, Hot Deformation Behavior of Cu–Fe–P Alloys During Compression at Elevated Temperatures, *J. Mater. Process. Technol.*, 2009, **209**, p 2892–2896. <https://doi.org/10.1016/j.jmatprotec.2008.06.048>
- G. Shi, X. Chen, H. Jiang, Z. Wang, H. Tang and Y. Fan, Strengthening Mechanisms of Fe Nanoparticles for Single Crystal Cu–Fe Alloy, *Mater. Sci. Eng. A*, 2015, **636**, p 43–47. <https://doi.org/10.1016/j.msea.2015.03.081>
- H.G. Kim, S.Z. Han, K. Euh and S.H. Lim, Effects of C Addition and Thermo-Mechanical Treatments on Microstructures and Properties of Cu–Fe–P Alloys, *Mater. Sci. Eng. A*, 2011, **530**, p 652–658. <https://doi.org/10.1016/j.msea.2011.10.041>
- Q. Dong, M. Wang, L. Shen, Y. Jia and Z. Li, Diffraction Analysis of α -Fe Precipitates in a Polycrystalline Cu–Fe Alloy, *Mater. Charact.*, 2015, **105**, p 129–135. <https://doi.org/10.1016/j.matchar.2015.05.012>
- I. Svinolobova, P. Ostrik and A. Kovzik, Properties of Iron–Copper Master Alloy Powder, *Powder Metall. Met. Ceram.*, 1997, **36**, p 567–569.
- M. Roy and H. Verma, Mössbauer Studies of Fe–Cu Alloys Prepared by Electrodeposition, *J. Magn. Magn. Mater.*, 2004, **270**, p 186–193. <https://doi.org/10.1016/j.jmmm.2003.08.017>
- S. Sheibani, S. Heshmati-Manesh and A. Ataie, Synthesis of Nano-Crystalline Cu–Cr Alloy by Mechanical Alloying, *Int. J. Modern Phys. Conf. Series*, 2012, **5**, p 496–501. <https://doi.org/10.1142/S2010194512002395>
- H. Ino, K. Hayashi, T. Otsuka, D. Isobe, K. Tokumitsu and K. Oda, Appearance of Ferromagnetism in fcc Solid Solutions of Binary and Ternary Fe–Cu-Based Systems Prepared by Mechanical Alloying Technique, *Mater. Sci. Eng. A*, 2001, **304**, p 972–974.
- Z. Chen, F. Liu, H. Wang, W. Yang, G. Yang and Y. Zhou, Formation of Single-Phase Supersaturated Solid Solution Upon Solidification of Highly Undercooled Fe–Cu Immiscible System, *J. Cryst. Growth*, 2008, **310**, p 5385–5391. <https://doi.org/10.1016/j.jcrysgro.2008.08.060>
- Z. Chen, F. Liu, X. Yang, C. Shen and Y. Fan, Analysis of Controlled-Mechanism of Grain Growth in Undercooled Fe–Cu Alloy, *J. Alloy. Compd.*, 2011, **509**, p 7109–7115.
- K. Nowakowska-Langier, R. Chodun, R. Nietubyc, R. Minikayev and K. Zdunek, Dependence of the Specific Features of Two PAPVD Methods: Impulse Plasma Deposition (IPD) and Pulsed Magnetron Sputtering (PMS) on the Structure of Fe–Cu Alloy Layers, *Appl. Surf. Sci.*, 2013, **275**, p 14–18. <https://doi.org/10.1016/j.apsusc.2013.01.190>
- U. Sarac and M.C. Baykul, Comparison of Microstructural and Morphological Properties of Electrodeposited Fe–Cu Thin Films with Low and High Fe: Cu Ratio, *Adv. Mater. Sci. Eng.*, 2013, **2013**, p 1–7. <https://doi.org/10.1155/2013/971790>
- Y. Yang, D. Wang, J. Lin, G. Lin and J. Ma, Evolution of Structure and Fabrication of Cu/Fe Multilayered Composites by a Repeated Diffusion-Rolling Procedure, *Mater. Des.*, 2015, **85**, p 635–639. <https://doi.org/10.1016/j.matdes.2015.07.082>
- P. Shingu, K. Ishihara, A. Otsuki and I. Daigo, Nano-Scaled Multi-Layered Bulk Materials Manufactured by Repeated Pressing and Rolling in the Cu–Fe System, *Mater. Sci. Eng. A*, 2001, **304**, p 399–402.
- D.J. Fray, T.W. Farthing, G.Z. Chen, Removal of Oxygen from Metal Oxides and Solid Solutions by Electrolysis in a Fused Salt, PCT Patent, WO9964638, (1998)
- K.S. Mohandas and D.J. Fray, FFC Cambridge Process and Removal of Oxygen from Metal–Oxygen Systems by Molten Salt Electrolysis: An Overview, *Trans. Indian Inst. Met.*, 2004, **57**, p 579–592.
- E. Gordo, G.Z. Chen and D.J. Fray, Toward Optimisation of Electrolytic Reduction of Solid Chromium Oxide to Chromium Powder in Molten Chloride Salts, *Electrochim. Acta*, 2004, **49**, p 2195–2208. <https://doi.org/10.1016/j.electacta.2003.12.045>
- L. Dai, S. Wang, Y.-H. Li, L. Wang and G.-J. Shao, Direct Electrochemical Preparation of CeCo_5 Alloy from Mixed Oxides, *Trans. Nonferrous Met. Soc. China*, 2012, **22**, p 2007–2013. [https://doi.org/10.1016/S1003-6326\(11\)61421-0](https://doi.org/10.1016/S1003-6326(11)61421-0)
- B. Zhao, L. Wang, L. Dai, G. Cui, H. Zhou and R. Kumar, Direct Electrolytic Preparation of Cerium/Nickel Hydrogen Storage Alloy Powder in Molten Salt, *J. Alloy. Compd.*, 2009, **468**, p 379–385. <https://doi.org/10.1016/j.jallcom.2008.01.074>
- Z. Yong, M. Meng, W. Dihua, J. Kai, H. Xiaohong, J. Xianbo and G.Z. Chen, Electrolytic Reduction of Mixed Solid Oxides in Molten Salts for Energy Efficient Production of the TiNi Alloy, *Chin. Sci. Bull.*, 2006, **51**, p 2535–2540. <https://doi.org/10.1007/s11434-006-2105-1>
- T. Örs, S. Tan, T. Öztürk and I. Karakaya, Synthesis of Fe–4.6 wt% B Alloy via Electro-Deoxidation of Mixed Oxides, *J. Mater. Sci.*, 2009, **44**, p 3514–3519. <https://doi.org/10.1007/s10853-009-3474-z>
- K. Yasuda, T. Nohira and Y. Ito, Effect of Electrolysis Potential on Reduction of Solid Silicon Dioxide in Molten CaCl_2 , *J. Phys. Chem. Solids*, 2005, **66**, p 443–447. <https://doi.org/10.1016/j.jpcs.2004.06.037>
- W. Xiao, X. Jin, Y. Deng, D. Wang, X. Hu and G.Z. Chen, Electrochemically Driven Three-Phase Interlines into Insulator Compounds: Electroreduction of Solid SiO_2 in Molten CaCl_2 , *ChemPhysChem*, 2006, **7**, p 1750–1758. <https://doi.org/10.1002/cphc.200600149>
- M. Ma, D. Wang, W. Wang, X. Hu, X. Jin and G.Z. Chen, Extraction of Titanium from Different Titania Precursors by the FFC Cambridge Process, *J. Alloy. Compd.*, 2006, **420**, p 37–45. <https://doi.org/10.1016/j.jallcom.2005.10.048>
- G. Li, X. Jin, D. Wang and G.Z. Chen, Affordable Electrolytic Ferrotitanium Alloys with Marine Engineering Potentials, *J. Alloy. Compd.*, 2009, **482**, p 320–327. <https://doi.org/10.1016/j.jallcom.2009.04.007>
- K. Yasuda, T. Nohira, K. Takahashi, R. Hagiwara and Y.H. Ogata, Electrolytic Reduction of a Powder-Molded SiO_2 Pellet in Molten CaCl_2 and Acceleration of Reduction by Si Addition to the Pellet, *J. Electrochem. Soc.*, 2005, **152**, p D232–D237. <https://doi.org/10.1149/1.2103947>
- M. Ojaghi-Ilkchi and H. Assadi, Modelling of Electroreduction of Porous Oxides in Molten Salt, *Comput. Mater. Sci.*, 2012, **53**, p 1–5. <https://doi.org/10.1016/j.commatsci.2011.08.002>

Publisher's Note Springer Nature remains neutral with regard to jurisdictional claims in published maps and institutional affiliations.